Covalent Bond Fragmentation Suitable To Describe Solids in the Fragment Molecular Orbital Method

Dmitri G. Fedorov,*,† Jan H. Jensen,‡ Ramesh C. Deka,§ and Kazuo Kitaura†,||

Research Institute for Computational Sciences, National Institute of Advanced Industrial Science and Technology, 1-1-1 Umezono, Tsukuba, Ibaraki 305-8568, Japan, Department of Chemistry, University of Copenhagen, 2100 Copenhagen, Denmark, Department of Chemical Sciences, Tezpur University, Napaam, Tezpur 784028, Assam, India, and Graduate School of Pharmaceutical Sciences, Kyoto University, Sakyo-ku, Kyoto 606-8501, Japan

Received: June 20, 2008; Revised Manuscript Received: August 7, 2008

To improve the accuracy of the fragment molecular orbital method (FMO), we introduce a new fragmentation scheme based on using frozen orbitals to describe fractioned bonds. By applying this scheme to a set of polyalanine systems of up to 40 residues for the α-helix and β-strand isomers, we established its accuracy, which is considerably improved compared to the original hybrid orbital projection method used for detaching bonds in FMO. For instance, at the two-body FMO expansion with the 6-311G* basis set, the error was typically reduced 2−4 times, and for 6-31G* the accuracy increase was even larger (10 times in terms of the maximum error). For the Trp-cage protein (PDB file 1L2Y) with many charged residues, a fairly large error was observed, which was shown to become small with a larger fragment size or at the three-body level. Consequently, we applied the new scheme to the adsorption of toluene and phenol on a faujasite zeolite, and we demonstrated that good accuracy can be achieved in reproducing ab initio results.

1. Introduction

Ab initio quantum-mechanical methods have been widely successful in describing various kinds of phenomena, owing to their generality and systematic improvability. By the appropriate choice of method, one can attain not only chemical[1] (1 kcal/mol) but often spectroscopic[2] (1 cm^{-1}) accuracy. The downside of ab initio methods is their steeply rising computational cost, which for the basic methods, such as restricted Hartree−Fock (RHF), scales as N^3, where N is the system size, and the scaling is even higher for correlated methods, being N^5 and N^7 for second-order Møller−Plesset perturbation theory (MP2) and coupled cluster [CCSD(T)], respectively. Recently a number of methods has been developed to reduce the computational costs of ab initio methods.[3−10]

An alternative approach is taken by fragment-based methods, which recently have been extensively reviewed.[11] The system is divided into pieces (fragments); typically ab initio calculations of fragments are performed, and hence the total properties are constructed, such as the energy or its gradient. These methods not only offer a very considerable reduction of the computational costs but also allude to the chemical building blocks in larger systems, such as residues taken as fragments, and provide details of the interaction and other properties of these fragments-in-molecules. However, the common need for manual manipulations, the lack of easy-to-use software to set up the calculations, and the necessity for long-term improvement have reduced many of the fragment-based approaches to a brief method development without consequent practical applications.

The fragment molecular orbital method (FMO) was introduced by Kitaura et al.[12] in 1999 and remains one of the actively developed fragment-based methods.[13] The distinctive features of FMO are the inclusion of the electrostatic field from the whole system into each individual fragment calculation and the use of systematic many-body expansion[14] to include interfragment interaction. Most common wave functions have been incorporated into FMO,[15−23] permitting one to describe various kinds of processes. The method is efficiently parallelized on large PC clusters[24] and vector computers (the Earth simulator),[25] making it suitable for efficient use of ever-growing computational power.

In addition to a very extensive method development, FMO has been applied to a large number of chemical processes, which can be divided into the following groups: (a) protein−ligand binding,[26,27] (b) protein−DNA interaction,[28] (c) explicit solvation,[29,30] (d) enzymatic reactions,[31] and (e) excited states in proteins.[32−35] Geometry optimizations[36] and molecular dynamics[37,38] simulations can be performed with FMO. The method was implemented into the freely distributed ABINIT-MP[13b] and GAMESS[39] software and made readily available to the end user through the development of the free graphical user interface Facio.[40]

Quantum-mechanical studies of solids and surfaces frequently rely on a cluster model,[41−43] which may be well suited for considering a defect in the periodicity, but the edge effects resulting from the surface truncation can be significant and sometimes even change the qualitative picture. At present, a common approach to quantum-mechanical studies of surface chemistry is via the ONIOM method,[44,45] or other somewhat similar schemes, all of which share the feature of describing a part of the system with quantum mechanics and the rest with molecular mechanics (MM). In particular, integrated molecular orbital (MO) and MM method (IMOMM)[46] and its surface version (SIMOMM)[47−49] have been suggested. Among the fragment-based or similar approaches, the elongation[50,51] and the incremental[9,52] methods have been applied to polymers and covalent crystals. Alternatively, for periodic systems one can

* Corresponding author: e-mail d.g.fedorov@aist.go.jp.
† National Institute of Advanced Industrial Science and Technology.
‡ University of Copenhagen.
§ Tezpur University.
|| Kyoto University.

10.1021/jp805435n CCC: $40.75
Published on Web 10/23/2008

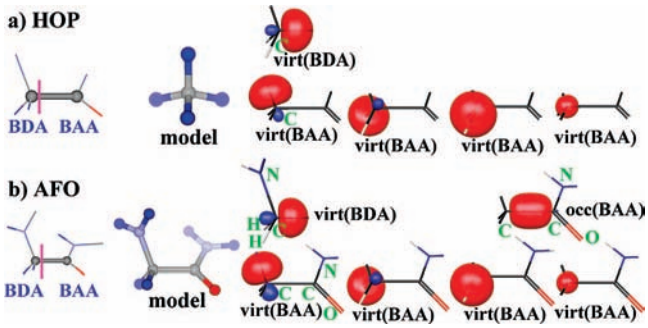

Figure 1. Fragmentation schemes used in FMO. (a) Original HOP; (b) AFO from this work, shown for the C−C bond adjacent to a peptide bond (for residues other than glycine, one hydrogen adjacent to BDA is replaced by -CH_3). The two atoms involved in the detached bond (BDA and BAA) are shown divided by the magenta line indicating the fragmentation. The model system used for the hybrid (HOP) or frozen (AFO) orbital construction is shown next. The actual virtual (projected out of the Fock space) and occupied (frozen) orbitals (6-31G*) are plotted for the BDA and BAA fragments, as indicated under each orbital [for example, virt(BAA) is a virtual orbital projected out from the BAA fragment]. The green atomic symbols show the atoms used in the orbital expansion over atomic orbitals. All virtual orbitals are strongly (AFO) or completely (HOP) localized on the BDA. The occupied orbital in AFO is localized between the BDA and BAA.

also utilize some quantum-mechanical methods (frequently density functional theory, or DFT) with periodic boundary conditions.[53]

The fragmentation process[13a] in FMO is in general suitable for detaching single covalent bonds when those with strong electron delocalization are avoided, such as the peptide bond, and the following bonds have been detached in the applications so far: C−C,[12] C−O,[23] Si−Si,[54] and Si−O.[54] Although it was hoped[54] that, with successful tests of Si−O fragmentation accuracy on simple linear model systems, one could now apply FMO to zeolites, no application of FMO to solids or surfaces has been published so far, to the best of our knowledge. The reason for this lies partially in the fragmentation scheme used in FMO, and now we suggest an alternative one, which will be shown below to be suitable for the computation of solids and should be applicable to surfaces as well.

Zeolites are industrially important microporous crystalline materials that possess the unique property in functioning as shape-selective catalysts in many reactions.[55] The acidic form of faujasite zeolites has been found to be significantly active in catalytic cracking of hydrocarbons in the petrochemical industry. Moreover, its supercage with a diameter of approximately 13 Å can be considered as a catalytic microreactor for the reactions of bulky molecules, including alkylation of toluene and phenol.[56,57] The protonated form of faujasite zeolites has been used as an eco-friendly catalyst in the liquid-phase *tert*-butylation of toluene for obtaining 4-*tert*-butyltoluene, which is an intermediate product for fine chemicals.[55] The products formed by alkylation of phenol are used as important raw intermediates for the synthesis of drugs, resins, pharmaceuticals, and dyes. In this paper we investigate the adsorption behavior of toluene and phenol in the acidic form of a faujasite zeolite by the FMO method.

2. Computations

2.1. Methodology. The original[13a] fragmentation scheme used in FMO is described below, where for the sake of clarity we assume a C−C bond (see Figure 1). Two electrons from a detached bond are assigned to one fragment and none to the other. Thus, the bond fragmentation is performed at an atom, not midway between the two atoms forming a bond, and this atom is referred to as the bond detached atom (BDA). The other atom on which the fractioned bond is retained is referred to as the bond attached atom, or BAA. BDA keeps all other electrons except the one which is assigned to the other side (BAA) of the detached bond, and in order to force the electron density on BDA not to occupy the bond region (which is taken up by the other fragment), the hybrid orbital projection technique is used, which is abbreviated HOP.[58] It is rather easy to accomplish this by use of the sp^3 hybrid orbitals (obtained from a preliminary calculation of CH_4), by shifting the orbital energies corresponding to the bond orbital (the sp^3 orbital on BDA, which points out toward BAA) to a large value, given by B below (typically, 10^6 au). The projection operator has the following form:

$$P = B\sum_{i=1}^{N_P} |\phi_i^h\rangle\langle\phi_i^h| \qquad (1)$$

where φ_i^h are hybrid orbitals (put on all BDAs) to be projected out and N_P is their total number. For the case of one single detached bond (see Figure 1), and the fragment, which does not include the bond (BDA fragment), one projects just a single hybrid orbital describing the bond ($N_P = 1$). For the detached bond including the fragment on the other side (BAA fragment), one projects out 1s and the other three sp^3 orbitals on the BDA except the one describing the bond ($N_P = 4$). In general, there are several bonds to be treated and N_P varies.

On the BAA fragment, one has to place a pseudoatom in the place of BDA, in order to have the carbon basis functions to describe the bond. For the purpose of a meaningful pair interaction analysis, one proton from BDA is also formally moved to the pseudoatom, which does not alter the total properties, since such a proton reassignment does not change the Coulomb field acting upon the fragment (because all nuclei contribute to it in FMO, from the particular fragment as well as from all other fragments). Similarly, one has to apply the projection operator to the pseudoatom on the BAA side to avoid its falling, for instance, into 1s orbital on C.

The projection operator technique succeeds in detaching the bond, and it leaves considerable freedom to the electron density distribution on both BDA and BAA as to how to adjust to the total electronic state in fragments and their pairs (dimers), under the restriction of not encroaching upon each other's electron levels of the BDAs. For proteins, where the fragmentation points (at Cα atoms adjacent to peptide bonds) are far from each other, the HOP scheme works quite well, as was extensively proved for various wave functions and basis sets[11] by comparing the total properties to ab initio calculations. Now, the problem occurs when this scheme is taken to surfaces or crystals, because the three-dimensional network of covalent bonds makes it practically impossible to avoid detaching close bonds.

While the HOP scheme does detach the bond in the desired way as far as the *particular* bond is concerned, there are two sources of problems when there are other close fractioned bonds. One is the polarization of the bond on the BAA side by other detached bonds. Another is the unphysical interfragment (and, possibly, intrafragment) charge transfer resulting from this strong polarizing environment. Thus, the pair corrections, which in FMO eliminate the fragmentation artifacts and introduce the interfragment interaction, are not good enough when applied to solids and surfaces.

The idea of employing frozen orbitals for the covalent bond division is very extensively used in the quantum mechanics/

molecular mechanics (QM/MM) hybrid approaches.[59,60] Now we apply these ideas to the fragmentation in FMO by taking advantage of the particular scheme developed for the effective fragment method (EFP) [61,62] by Kairys and Jensen,[63] in which it is shown that the frozen orbital treatment can be practically performed in the form of the Fock matrix **F** transformation, and we now apply it to fragments and their pairs as shown below. Note that in FMO one is interested not in one but in both sides of the detached bond, and similar to the HOP scheme, one has to project not only the appropriate occupied but also the virtual orbitals, which corresponds to removing the undesired orbital from the Fock space by shifting it with the *B* constant in HOP.

$$\widetilde{\mathbf{F}} = \mathbf{U}^{\dagger}\mathbf{F}\mathbf{U} \tag{2}$$

$$\widetilde{\widetilde{F}}_{ij} = \begin{cases} B & \text{for } i = j \text{ and } M_o < i \le M \\ 0 & \text{for } i \le M_o \text{ and } j > M_o \text{ or for } j \le M_o \text{ and } i > M_o \\ \widetilde{F}_{ij} & \text{otherwise} \end{cases} \tag{3}$$

$$\mathbf{F}' = \mathbf{S}\mathbf{U}\widetilde{\widetilde{\mathbf{F}}}(\mathbf{S}\mathbf{U})^{\dagger} \tag{4}$$

where **S** are overlap integrals and the matrix of the frozen orbitals **U** consists of M_o occupied followed by $M - M_o$ virtual frozen orbitals (see below), and the other vectors in **U** are computed as the orthogonal complement to the first *M* vectors. In constructing $\widetilde{\widetilde{\mathbf{F}}}$, the matrix elements of the transformed Fock matrix $\widetilde{\mathbf{F}}$ are copied with two exceptions, as shown above in eq 3: (a) the diagonal element of $\widetilde{\mathbf{F}}$ is replaced by the large universal constant $B = 10^6$ for the virtual frozen orbitals, corresponding to the HOP projection, and (b) the mixing of the occupied frozen orbitals and all other orbitals is prohibited ($\widetilde{\widetilde{F}}_{ij} = 0$). Finally, $\widetilde{\widetilde{\mathbf{F}}}$ is transformed back and $\mathbf{F}'$ replaces the Fock matrix **F** during SCF on each iteration.

It can be noted that only the occupied orbitals are frozen (as determined by prohibiting orbital mixing with the virtuals in the Fock matrix), whereas the virtual orbitals are given the freedom to mix; thus they are not frozen but simply projected out, similar to the HOP method. The real large difference from the original HOP fragmentation is thus in freezing the occupied orbitals (see Figure 1); there is also some small difference in the virtual projection, which is because (a) the model system is somewhat different, (b) the frozen orbital expansion is over several atoms versus only one in HOP, (c) the virtual AFOs are orthogonal, and (d) different localization schemes are often used.

A complication arises here as the HOP method applies only to the BDA basis functions, and in order to use it in practical calculations, one needs to supply a single set of sp^3 orbitals, which are localized for a model system (e.g., CH_4) and rotated as needed to match the bond direction in the actual system. Now we attempt to freeze the electron density, and it is not possible to meaningfully freeze it just on one atom for a simple model system (CH_4). The model system includes several atoms (typically, 11 or 14 for polypeptides), and it would be very tedious to enforce the required order of atoms in the real and model systems. In addition, one would have to enforce fixed bond lengths or angles, or else assume that the model system with some set of geometric parameters can describe well the actual atomic environment.

Thus we took a different approach, in which we generate the frozen orbitals on the fly for each given system, and this new fragmentation scheme in FMO is referred to as the adaptive frozen orbital (AFO) scheme. Adaptive implies their construction in the model system made for each fragmentation point found in a given system to be computed, with the geometric parameters of the real system. Consequently, in FMO calculations these orbitals are frozen or used for projection. This is rather convenient from the practical viewpoint, as the only information one has to supply to perform calculations is the pairs of atoms specifying the fragmentation points, and all kinds of bonds can be fragmented, such as Si−O bonds, subject to the general practice in FMO (single bonds without a strong electron delocalization).

Practically, the algorithm implemented in GAMESS to construct the model system works as follows. For a given fragmentation point, two atoms (BDA and BAA) are specified. Then all atoms covalently bound to either BDA or BAA are identified from the set of atomic coordinates. Next, hydrogen caps are added as needed to all atoms thus chosen, by use of a predefined X−H set of distances for atoms X.[64] This forms the model system, for which RHF[14] (or DFT)[65] calculations are performed, and molecular orbitals are localized with the Edmiston−Ruedenberg scheme.[66]

Next, one has to identify the orbitals that describe the bond and other orbitals on the BDA. This is done also completely automatically, based on the overlap criterion $L_{i\alpha}$ related to the Mulliken charge of the molecular orbital *i* computed just for atom α:

$$L_{i\alpha} = \sum_{\mu\nu\in\alpha} C^{*}_{\mu i} S_{\mu\nu} C_{\nu i} \tag{5}$$

where **C** contains the MO coefficients, **S** is the overlap matrix, and μ, ν run over atomic orbitals. A large value of $L_{i\alpha}$ is taken to imply that orbital *i* is localized on α, and the required number of orbitals (e.g., 1s and four sp^3) are chosen on the basis of the largest values of $L_{i\alpha}$ where α is BDA ($L_{i\beta}$, where β is BAA, is also used to identify the orbital describing the bond to be detached).

Finally, the orbital coefficients for all necessary orbitals (e.g., sp^3 and 1s for C) are stored for a set of atoms in the close vicinity of a detached bond (Figure 1). Practically, we save coefficients only for atoms covalently bound to BDA (one side) or to BAA (the other side). As found by the previous study,[62] one can simply truncate other coefficients without a more complicated basis-set transformation. Then, for each fragment and fragment pair, these orbital coefficients are put into the matrix **U** and orthonormalized by the Gram−Schmidt procedure.

The AFO orbitals were thus used in individual fragment and fragment pair calculations, following the standard FMO scheme[13a] of obtaining the total properties of the system in the many-body expansion:

$$E^{\mathrm{FMO3}} = \sum_{I}^{N} E_I + \sum_{I>J}^{N} (E_{IJ} - E_I - E_J) + \sum_{I>J>K}^{N} [(E_{IJK} - E_I - E_J - E_K) - (E_{IJ} - E_I - E_J) - (E_{JK} - E_J - E_K) - (E_{KI} - E_K - E_I)] + \cdots \tag{6}$$

where E_I, E_{IJ}, and E_{IJK} are the monomer (fragment), dimer (fragment pair), and trimer (fragment triple) energies, respectively, and all *n*-mers ($n = 1, 2, 3$) in FMO are computed in the Coulomb field due to the rest of the fragments. The above E^{FMO3} energy corresponds to the three-body expansion (FMO3), which can be truncated at the two-body level FMO2 (by removal of the last sum), whose energy is denoted by E^{FMO2}. The total

properties such as $E^{\mathrm{FMO}n}$ can be directly compared to the total RHF energy E^{RHF}without fragmentation.

The above scheme permits the following choices regarding the definition of the orbitals: (a) the model system size and the particular way of its construction, (b) the number of orbitals to freeze, and (c) the size of the AFO expansion in terms of the atomic orbitals. We performed elaborate tests to find the optimum choice for FMO, and the results indicate the following. The model system size cannot be too small, and the one indicated in Figure 1 is the smallest to gain reasonable results. Further increase in the size of the model system does not lead to a noticeable improvement in the accuracy.

Only one orbital can be frozen in FMO. This is contrary to the typical scenario in QM/MM or EFP calculations, when usually more orbitals are frozen.[63] FMO differs from QM/MM in describing the whole system quantum-mechanically, and it is necessary to describe both sides of a fractioned bond well. Freezing more orbitals very strongly restricts the proper polarization of the system, increasing the error manifold. The AFO expansion should be at least over the atoms bonded to the BDA and BAA (e.g., four atoms for a peptide bond; see Figure 1). A further increase imposes stronger restrictions upon the variational freedom in SCF and appears to worsen the accuracy.

Summarizing, we observe that the intuitive supposition, that the best choice of the frozen orbitals would be by the localized orbitals obtained for the whole system, appears to be wrong for FMO. Fragments in FMO provide the basis for the many-body corrections (from pair and triple calculations), and especially for small basis sets, the full relaxation of the fragments permitting their unrestricted polarization provides a nearly perfect set of fragment electronic densities, with the caveat that the fractioned bonds should not be near each other. Thus, for a systems like polypeptides and small basis sets (e.g., STO-3G), fully relaxed orbitals in the corresponding fragments describing the fractioned bonds appear to be a better choice than frozen orbitals even if the latter were generated for the whole system. This can be seen from the submillihartree accuracy of FMO/HOP for the STO-3G basis set.[14] The fully relaxed set of orbitals (i.e., the HOP scheme) does lead to fairly considerable errors with large basis sets (6-311G* and up) or when fractioned bonds are too near, as shown below in zeolite calculations.

2.2. Calculation Details. The AFO fragmentation scheme was implemented in GAMESS,[39] which was used for all computations in this work. Model systems are constructed before any other fragment calculations in FMO start, and the appropriate molecular orbital coefficients for the AFOs are stored. These calculations are parallelized in the two-level hierarchical scheme,[24] distributing the model systems to groups of CPUs and the particular workload for a model system among the CPUs, similar to the FMO parallelization. The SCF and integral accuracy in ab initio calculations was increased to match the default values in FMO. Spherical d-orbitals (5d) were used throughout.

Facio[40] was employed to set up the input files for the AFO fragmentation. Practically, one only needs to specify pairs of atoms defining the fragmentation points, by use of its graphical user interface, and choose the computation level (wave function and basis set), and the rest is done automatically. The orbitals visualized in Figure 1 were plotted with MacMolPlot.[67]

When discussing the accuracy below, the following definitions of the errors were used:

$$\Delta E^n = E^{\mathrm{FMO}n} - E^{\mathrm{RHF}}$$
$$\Delta D^n = |\mathbf{D}^{\mathrm{FMO}n} - \mathbf{D}^{\mathrm{RHF}}|/3 \quad (7)$$

where $\mathbf{D}^{\mathrm{FMO}n}$ and $\mathbf{D}^{\mathrm{RHF}}$ are the dipole moment vectors for FMOn ($n = 2, 3$) and RHF, respectively. The dipole moment is of particular interest, as the AFO scheme can be expected to affect the polarization of the system. Just looking at the energy may be misleading, as error cancelation can hide the problems.

To discuss the binding energy for the zeolite adsorption, we divided it into the following contributions:

$$\Delta E_{\mathrm{bind}} = E_{\mathrm{AB}} - E_{\mathrm{A}}^0 - E_{\mathrm{B}}^0 = \Delta E_{\mathrm{int}}^{\mathrm{AB}} + E_{\mathrm{AB}}^{\mathrm{A}} + E_{\mathrm{AB}}^{\mathrm{B}} - E_{\mathrm{A}}^0 - E_{\mathrm{B}}^0 = \Delta E_{\mathrm{int}}^{\mathrm{AB}} + \Delta E_{\mathrm{destab}}^{\mathrm{A}} + \Delta E_{\mathrm{destab}}^{\mathrm{B}}$$
$$\Delta E_{\mathrm{destab}}^{\mathrm{A}} \equiv E_{\mathrm{AB}}^{\mathrm{A}} - E_{\mathrm{A}}^0 \quad (8)$$
$$\Delta E_{\mathrm{destab}}^{\mathrm{B}} \equiv E_{\mathrm{AB}}^{\mathrm{B}} - E_{\mathrm{B}}^0$$

where A stands for zeolite and B for guest.

The total FMO energy of the zeolite−guest complex E_{AB} is divided into the zeolite−guest interaction energy $\Delta E_{\mathrm{int}}^{\mathrm{AB}}$ and the partial energy of zeolite $E_{\mathrm{AB}}^{\mathrm{A}}$ and guest $E_{\mathrm{AB}}^{\mathrm{B}}$ inside the complex. E_{A}^0 and E_{B}^0 are the energies of zeolite and guest, respectively, in their free state. Thus, the destabilization energies $\Delta E_{\mathrm{destab}}^{\mathrm{A}}$ and $\Delta E_{\mathrm{destab}}^{\mathrm{B}}$ include the deformation energy[68] (the energy related to the structure change during adsorption) and the destabilization component[69] of the polarization in the complex (since the energies $E_{\mathrm{AB}}^{\mathrm{A}}$ and $E_{\mathrm{AB}}^{\mathrm{B}}$ correspond to the fully polarized state in the complex in FMO). The stabilization component of the polarization is included into $\Delta E_{\mathrm{int}}^{\mathrm{AB}}$ along with other interactions, such as the charge transfer.

Charge transfer often serves as a quality criterion in FMO, because at the monomer level no charge transfer is allowed, and large charge transfer values in the dimer calculations indicate that monomers, which determine the electrostatic field in FMO and in general serve as the basis for the pair corrections, do not represent well the electronic state of the system. We defined the following value to analyze the accuracy:

$$\Delta Q = \sum_{I>J}^{N} |\Delta Q_{IJ}| \quad (9)$$

where ΔQ_{IJ} is the charge transfer[69] between fragments I and J. We note that there is some ambiguity in the definition of ΔQ_{IJ} for the connected dimers (those between which at least one covalent bond is detached), and it is meaningful to look at ΔQ differences.

The timings for AFO are very similar to those of HOP, which were published in detail elsewhere.[70] The AFO construction takes little time, although it does involve a two-electron integral transformation for the occupied orbitals only.[66] In addition, AFO requires fewer monomer calculations, as the monomer densities converge faster with it (which is a direct consequence of freezing the detached bond orbitals.)

3. Results and Discussion

3.1. Application to Polypeptides. We calculated linear capped polyalanine chains CH_3CO-$(Ala)_n$-$NHCH_3$ for the α-helix [denoted as α-$(ALA)_n$] and the β-strand [denoted as β-$(ALA)_n$] with $n = 10$, 20, and 40 residues. In addition, we also computed the small synthetic Trp-cage protein (PDB file 1L2Y), consisting of 304 atoms. The structures used for the calculations were taken from our previous work.[70] Two fragment sizes, one and two residues per fragment, as well as two basis sets (6-31G* and 6-311G*) were compared (for the Trp-cage

TABLE 1: Accuracy of the FMOn−RHF Methods (HOP and AFO) versus ab Initio RHF[a]

		6-31G*				6-311G*			
method	m	ΔE^2	ΔE^3	ΔD^2	ΔD^3	ΔE^2	ΔE^3	ΔD^2	ΔD^3
					α-$(ALA)_{10}$				
HOP	1	−4.8	0.3	0.23	0.01	−14.6	−2.0	0.79	0.08
AFO	1	0.4	0.3	0.23	0.02	−3.2	0.4	0.35	0.02
HOP	2	−1.0	0.0	0.02	0.00	−5.5	−0.1	0.21	0.02
AFO	2	−0.8	0.0	0.04	0.01	−1.7	0.0	0.10	0.02
					β-$(ALA)_{10}$				
HOP	1	−6.6	−0.1	0.19	0.04	−11.2	0.1	0.33	0.01
AFO	1	−0.1	−0.2	0.41	0.11	−5.3	− 0.6	0.70	0.23
HOP	2	0.0	0.0	0.02	0.00	0.1	0.0	0.05	0.01
AFO	2	0.1	0.0	0.06	0.01	0.2	0.0	0.08	0.01
					α-$(ALA)_{20}$				
HOP	1	−12.0	1.2	0.55	0.03	−38.0	−5.5	2.20	0.34
AFO	1	−0.7	0.5	0.46	0.05	−9.7	0.5	0.95	0.16
HOP	2	−3.0	0.1	0.02	0.05	−15.9	−0.3	0.57	0.06
AFO	2	−2.4	− 0.1	0.03	0.01	−5.2	−0.2	0.23	0.04
					β-$(ALA)_{20}$				
HOP	1	−14.6	− 0.2	0.50	0.15	−24.8	0.4	0.83	0.09
AFO	1	−0.1	−0.3	0.93	0.29	−11.5	−1.4	1.58	0.57
HOP	2	0.0	0.0	0.07	0.02	0.2	0.1	0.17	0.04
AFO	2	0.2	0.0	0.16	0.04	0.5	0.1	0.23	0.05
					α-$(ALA)_{40}$				
HOP	1	−27.2	2.8	1.27	0.15	−87.1	−12.5	5.17	0.93
AFO	1	−3.1	1.0	0.86	0.06	−23.7	0.7	2.17	0.43
HOP	2	−7.2	0.4	0.08	0.14	−37.5	−0.7	1.29	0.12
AFO	2	−5.6	−0.1	0.05	0.10	−12.5	−0.6	0.44	0.04
					β-$(ALA)_{40}$				
HOP	1	−30.7	−0.3	1.13	0.38	−51.8	1.2	1.87	0.28
AFO	1	−0.1	−0.7	2.00	0.65	−23.9	−3.0	3.33	1.25
HOP	2	0.0	0.0	0.19	0.07	0.6	0.2	0.42	0.13
AFO	2	0.5	0.1	0.37	0.10	1.1	0.3	0.53	0.14
					PDB file 1L2Y				
HOP	1	−4.6	0.3	0.32	0.03	−35.9	−5.2	0.51	0.03
AFO	1	10.8	0.2	0.31	0.01	−1.9	−7.6	1.18	5.04
HOP	2	−0.2	−0.1	0.15	0.02	−11.4	−0.2	0.25	0.04
AFO	2	1.3	−0.1	0.14	0.02	−1.4	−0.1	0.29	0.04

[a] In terms of the total energy ΔE^n (kilocalories per mole) and dipole moment ΔD^n (debyes), for the m residues per fragment division of capped polyalanine with 10, 20, and 40 residues.

protein, we added diffuse functions on all carboxyl groups). The results are summarized in Table 1.

For both isomers of $(ALA)_n$, the AFO scheme delivered a very much improved accuracy of FMO2 in the energy with respect to ab initio RHF. For the 6-31G* basis set, the FMO2/AFO reproduces the full RHF energies within 3.1 kcal/mol error, compared to 30.7 kcal/mol errors of FMO2/HOP. The relative stability of the two isomers is very well reproduced by the FMO2/AFO method, whereas the original HOP scheme overestimated the stability of the α-helix. For instance, for two residues per fragment and $n = 40$, HOP has an error of 7.2 kcal/mol, whereas AFO has an error of only 0.5 kcal/mol.

At the three-body level, AFO and HOP deliver similar accuracy for the 6-31G* basis set, with the largest errors being 1.0 and 2.8 kcal/mol, respectively. Doubling the fragment size has a very large accuracy improvement for HOP, while for AFO the effect is less pronounced, perhaps because the calculations for the smaller fragment size already are quite accurate. For dipole moments at the 6-31G* level, both AFO and HOP schemes have similar errors. The dipole moment of the α-helix is overestimated by the HOP method and is considerably improved by AFO; for β-strand, the former method produces a somewhat better value.

Most observations on the accuracy remain the same when the basis set is increased to 6-311G*. The absolute error magnitude is larger compared to 6-31G*, but the FMO2/AFO method still reproduces the relative stability of the α-helix versus the β-strand within 2.2 kcal/mol for the one residue per fragment division. When the fragment size is increased to two residues, the β-strand total energy is nearly identical to the ab initio value, while the α-helix has a somewhat larger error (up to 12.5 kcal/mol). The HOP scheme has much larger errors in the energy than AFO at the FMO2 level. For FMO3, both schemes reproduce well the total RHF energies, almost exactly at the two residues per fragment level, but for one residue per fragment, HOP and AFO have maximum errors of 12.5 and 3.0 kcal/mol, respectively. The dipole moments at the 6-311G* level follow the trends for 6-31G*.

Summarizing the $(ALA)_n$ results, the energies are much improved by AFO compared to the original HOP, while for dipole moments the errors are similar and neither method appears to be systematically better than the other.

The small Trp-cage protein has five charged residues out of 20. As can be seen from Table 1, for 6-31G* and one residue per fragment, the original HOP had better accuracy (−4.6 vs 10.8 kcal/mol, respectively), and we also note the sign difference (AFO predicted a somewhat destabilized energy vs ab initio RHF, whereas HOP overstabilized the system). Going either to two residues per fragment or to FMO3 permitted a nearly exact reproduction of the ab initio results, with errors under 1.3 kcal/mol (again, AFO predicted a destabilized energy).

For the larger 6-311G* basis set, AFO delivered much more accurate energies than HOP, except at the FMO3 level with two residues per fragment, when both had comparable accuracy. However, the dipole moment in the AFO scheme had considerable errors. Both methods almost exactly reproduced the ab initio properties at the FMO3 level with two residues per fragment.

Pair interaction energy decomposition analysis (PIEDA)[69] gives the means to analyze the above results. As found by performing comparative tests, the original FMO with fully variational monomer density relaxation (HOP) exactly[69] describes the polarization of the system, and in AFO the polarization is somewhat reduced (i.e., underestimated) by the frozen fractioned bond orbitals. The main source of the FMO error is in the inclusion of coupling terms between the polarization, exchange, and charge transfer at the two- and three-body levels for FMO2 and FMO3, respectively.

What AFO accomplishes is the reduction of full polarization in FMO, and it is quite successful in balancing the omitted many-body terms (the coupling of polarization with other interactions) with the reduced polarization, as can be seen for the $(ALA)_n$ systems. However, in the case of highly polar systems, such as proteins, the reduced polarization in AFO leads to considerably larger errors compared to HOP, when medium-sized basis sets are used and the many-body terms are much less important than the proper polarization of the system. For large basis sets (6-311G*), these many-body terms play a very important role, comparable to the polarization itself (it was often argued[71] that the polarization in the energy decomposition analysis,[72] which is a predecessor of FMO, becomes hardly distinguishable from charge transfer when large basis sets are used), and then the two schemes AFO and HOP may be competitive, although the latter is perhaps more reliable.

Thus, one can conclude that increasing the basis set size in the well-established series, such as from 6-31G* to 6-311G* or from cc-pVDZ to cc-pVTZ, results in larger charge transfer and coupling of charge transfer to polarization, which are introduced in FMO as two- and three-body corrections; to obtain good accuracy with these large basis sets, one has to increase

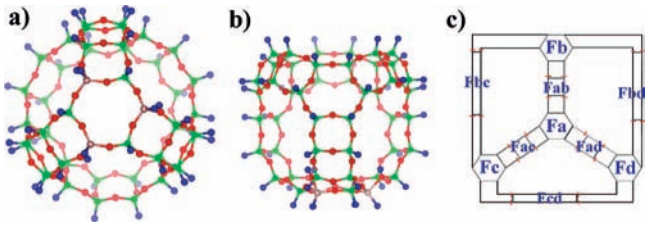

Figure 2. Faujasite zeolite (isomer 1). (a) Top view with the Al-containing 6-member ring in the center; (b) side view with this ring on the bottom. H, Si, O, and Al atoms are shown in blue, green, red, and magenta, respectively. (c) Basic fragmentation scheme of a faujasite zeolite, with red line showing detached bonds. Zeolite contains four 6-member rings, connected to each other by edges with three 4-member rings. There are 10 fragments encompassing four 6-member rings (*F*a, etc.) and six 4-member rings (*F*ab, etc.), as shown.

the fragment size and, depending on the desired accuracy, consider using the three-body expansion.

3.2. Application to Solids. As noted above, FMO with HOP cannot reproduce well the total properties of surfaces and covalent crystals, due to a high density of interacting fractioned bonds, because no caps are used in FMO to terminate detached bonds. To demonstrate the efficiency of AFO and compare it to HOP, we computed the adsorption of two small molecules (toluene and phenol) on a faujasite zeolite containing three Al atoms at the 6-member ring of the supercage in a faujasite zeolite, which was modeled by a 171-atom cluster (Figure 2). It should be noted that zeolites represent a rather difficult test system, since guest molecules enter pores in zeolites and interact with various parts of the inner surface. Studying processes on the surfaces may be easier.

First, we fully optimized the structure of zeolite and zeolite−guest complexes using ab initio RHF with the 6-31G* basis set. The optimized structure for zeolite without guests is of a nearly perfect C_3 symmetry (the C_3 axis is perpendicular to the Al-containing 6-member rings). Consequently, we defined a reaction coordinate and varied its values to obtain an energy profile, while fixing all other geometric parameters. Such a profile should be very useful in determining the reliability of energy evaluation by FMO, but it does not necessarily reproduce the actual binding mode. It should be noted that we did not compare various binding sites and conformations of zeolite. Instead, we chose one such site for each molecule, because our purpose here is to test FMO accuracy on a realistic system.

For a better test of FMO reliability, we took two isomers of a faujasite zeolite, denoted as 1 and 2 below. In the first isomer (Figure 2), three hydrogen atoms were attached to oxygens in the 4-member rings, adjacent to Al atoms. In the second isomer (Figure 3), the corresponding hydrogen atoms were attached to oxygen atoms on the 6-member ring containing Al atoms. The 4- and 6-member notation applies to the number of Si and Al atoms in a ring, which always includes an equal number of O atoms, so a 4-member ring stands for $(\text{-Si-O-})_4$. We used isomers 1 and 2 for the adsorption of toluene and phenol, respectively.

The adsorption site (Figure 4) for phenol is on the border between the Al-containing 6-member ring (the central part of *F*a) and an adjacent 4-member ring (in the direction of *F*ab). For toluene, it is also somewhat at the same location but is more separated from the Al site. Al atoms have formal charges of +1 and the acidic oxygen atoms bound to Al have a formal charge of −1. The Mulliken charges on Al and acidic oxygens are equal to the formal charges within about 16%. It should be noted that the presence of Al defects (Si substituted by Al) is the key factor in the catalytic activity of zeolites. Thus, this

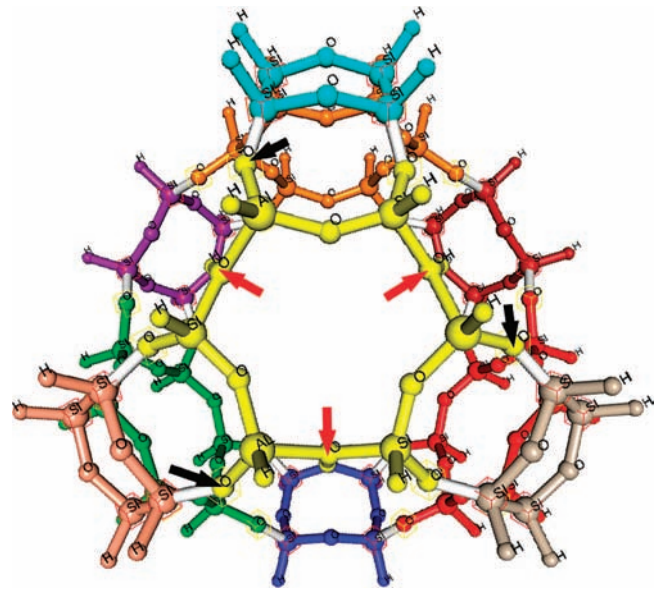

Figure 3. Fragmentation of a faujasite zeolite (isomer 2) in FMO at a glance. Atoms are colored by fragments. Yellow, red, light brown, and green fragments are the 6-member rings. The position of acidic oxygens in isomer 2 is shown by red arrows. In isomer 1, hydrogen atoms attached to those oxygens are moved to oxygen atoms indicated by black arrows.

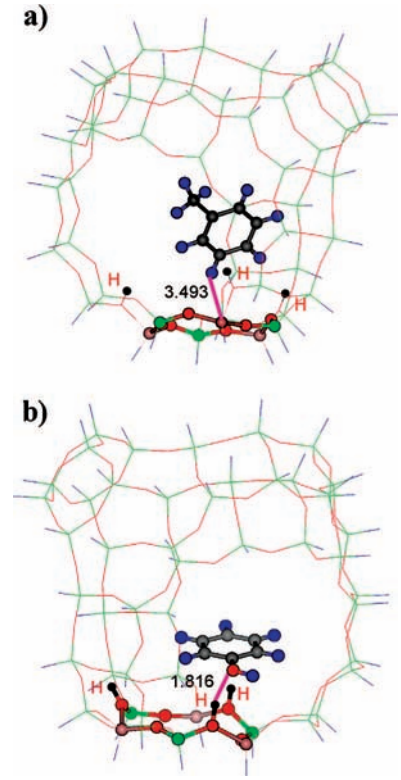

Figure 4. Adsorption of (a) toluene and (b) phenol on a faujasite zeolite (RHF/6-31G* optimized structures). The active site is shown with ball-and-stick models; the reaction coordinate is depicted with a violet stick, and the value at equilibrium is shown in angstroms. The Brønsted acidic hydrogens are shown as black spheres with a red atomic symbol (H).

system is polar to a large extent, presenting some difficulty for a proper description in the fragment-based methods; FMO seems advantageous as it properly includes the polarization due to self-consistent optimization of fragment densities in the total electrostatic field.

TABLE 2: Comparison of the Two Zeolite Isomers[a]

method	$\Delta\varepsilon_1$	$\Delta\varepsilon_2$	ΔE_{2-1}	ΔQ_1	ΔQ_2
AFO/*F*10	6.9	12.0	−12.2	0.61	0.63
AFO/*F*9a	6.1	9.5	−14.0	0.53	0.53
HOP/*F*10	180.4	192.6	−5.1	1.33	1.47
HOP/*F*9a	149.7	156.4	−10.6	1.25	1.35

[a] The two isomers are optimized with RHF/6-31G*) and are denoted by subscripts 1 (anionic oxygens on 4-member rings) and 2 (anionic oxygens on 6-member rings); all energies are in kilocalories per mole. $\Delta\varepsilon$ is the error in the FMO total energy vs ab initio RHF. ΔE_{2-1} is the relative stability of the two structures (the ab initio value is −17.4). ΔQ is the total interfragment charge transfer (au). *F*10 and *F*9a denote fragmentation schemes.

We tried several fragmentation schemes. The basic one denoted by *F*10 is shown schematically in Figure 2c and also in Figure 3, in which zeolite is divided into 10 fragments, and guest also forms a separate fragment. Another scheme is to combine *F*a and *F*ab into one fragment to have nine fragments in zeolite (*F*9a). This is done since the adsorption site is between *F*a and *F*ab and both are important. In the third scheme, we took *F*10 and added the guest to fragment *F*a, since the binding (adsorption) is of primary interest (fragmentation *F*9b). In the forth scheme, *F*8, we combined *F*a, *F*ab, and guest into one large fragment. It should be noted that since in FMO fragment pair calculations are performed, such fragment enlargement is not crucial but affects the total accuracy to a small degree. Also, the following discussion of the contributions of zeolite fragments involves some subjective definition of fragments, which is in some sense artificial; however, in chemistry one often deals with functional groups and such, supposing them to represent units to which some properties can be assigned, and our fragments are like that.

A comparison of the two isomers is given in Table 2. It can be seen that AFO provides a very close total energy compared to the ab initio RHF, whereas HOP gives a large systematic error ($\Delta\varepsilon$). The relative stability of the two isomers is reasonably described by AFO (the largest error being 3.4 kcal/mol), while HOP gave considerably larger errors (7.4 kcal/mol or more). The charge transfer values ΔQ are much larger for HOP compared to AFO. It can be noted that ΔQ_2 is larger than ΔQ_1, which is related to the larger error in the absolute energy $\Delta\varepsilon_2$ (compared to $\Delta\varepsilon_1$). For comparison, ΔQ in α-$(ALA)_{10}$ was 0.38 and 0.44 for AFO and HOP, respectively (6-31G*). We note that throughout this work we use the Mulliken atomic charges and define the interfragment charge transfer according to the computational scheme suggested for FMO earlier.[69]

The main source of charge transfer in all schemes is the electron density donation from the 6-member ring fragments (*F*a, *F*b, *F*c, and *F*d) into the adjacent 4-member ring fragments (*F*ab, etc). For Si-only and Al-containing 6-member rings, respectively, 0.04 and 0.08/0.09 e is transferred in AFO; for HOP, the corresponding values are 0.12 and 0.09/0.14 e. The two values for the Al-containing ring are given for the two isomers of the zeolite (isomer 1 has the smaller value in the pair). The relative stability of the two isomers is considerably better reproduced with AFO; for HOP, error cancelation results in fairly small errors. This is because the two isomers are not very different from each other.

Using a smaller number of fragments (*F*9a vs *F*10) gives better results. It should be noted that for zeolite without guests there are three nearly equivalent 4-member ring fragments (*F*ab, *F*ac, and *F*ad), and the addition of one to *F*a in *F*9a gives a partial improvement as far as the zeolite by itself is concerned, but this addition is important to describe the binding. The mostly electrostatic repulsive interaction between the 6-member ring fragments (*F*a, *F*b, *F*c, and *F*d) is very large: for each pair, about 30 and 50 kcal/mol in AFO and HOP, respectively. Since it is not accompanied by a charge transfer, it probably does not affect the accuracy, as pair calculations effectively take care of it.

TABLE 3: Guest−Zeolite Pair Interaction Energies ΔE, Charge Transfer ΔQ, and Separation R[a]

	toluene			phenol		
fragment	R (Å)	ΔQ (au)	ΔE (kcal/mol)	R (Å)	ΔQ (au)	ΔE (kcal/mol)
*F*a	2.47	−0.06	−8.4	1.82	−0.13	−21.0
*F*b	3.21	−0.02	−3.6	3.37	−0.01	−1.6
*F*c	4.54	0.00	0.0	6.46	0.00	0.7
*F*d	7.10	0.00	0.2	4.64	0.00	−0.6
*F*ab	3.50	−0.06	−3.4	3.01	−0.03	−1.8
*F*ac	4.27	−0.00	0.2	5.58	0.00	−0.9
*F*ad	5.95	0.00	0.2	3.91	0.00	−1.0
*F*bc	4.51	0.00	0.2	7.86	0.00	−0.1
*F*bd	7.11	0.00	0.1	7.05	0.00	0.1
*F*cd	10.33	0.00	−0.1	8.87	0.00	−0.1

[a] For a faujasite zeolite divided into 10 fragments (*F*10) in FMO-RHF/AFO with 6-31G*, at the minimum geometry. See Figure 2 for the fragment definition.

TABLE 4: Contributions to Binding Energies ΔE_{bind}[a]

	toluene	phenol
ΔE_{int}^{tot} (kcal/mol)	−14.5	−26.3
$\Delta E_{destab}^{guest}$ (kcal/mol)	1.5	3.1
$\Delta E_{destab}^{zeolite}$ (kcal/mol)	0.9	2.4
ΔE_{bind} (kcal/mol)	−12.1	−20.8

[a] Total guest−zeolite interaction (ΔE_{int}^{tot}), guest destabilization ($\Delta E_{destab}^{guest}$), and zeolite destabilization ($\Delta E_{destab}^{zeolite}$) are listed for a faujasite zeolite divided into 10 fragments (*F*10) in FMO-RHF/AFO with 6-31G*.

For analysis of the binding it is more convenient to use a larger number of fragments, so we summarized the interactions between zeolite and guest in Table 3 for the fragmentation scheme *F*10. One can see that the main contributor to the binding is the Al-containing 6-member ring fragment (*F*a), especially for phenol, which is natural because phenol is closer to zeolite (R) than toluene. Two other important sites can be seen for both guests: *F*b and *F*ab. As indicated above, the binding site is between *F*ab and *F*a, and it is not surprising that *F*ab has a larger interaction energy. *F*b is in fact also close to adsorbant molecules. A large charge transfer occurs between the guest and *F*a, as well as *F*ab and, to a smaller extent, *F*b. Larger charge transfer values indicate that it is more important to include *F*ab to the binding site (as in *F*9a) than *F*b, as far as FMO is concerned.

In Table 4, the FMO binding energies are decomposed into components for the adsorption of toluene and phenol, defined (eq 8) relative to the free state of zeolite isomers 1 and 2, respectively. A much larger interaction occurs in phenol, which is also more strongly destabilized by zeolite (and zeolite is more strongly destabilized by phenol).

The total binding energies for various fragmentation schemes are summarized in Table 5. Regarding the AFO and HOP comparison, the same trends are observed as discussed above for Table 2. HOP gives a very large absolute error in the total energies ($\Delta\varepsilon$), which due to the error cancelation mostly disappears, since the structure of zeolite and guest is not much deformed upon binding (otherwise HOP would give worse results). The importance of the binding site definition during

TABLE 5: Total Energy Errors $\Delta\varepsilon$ of FMO versus ab Initio RHF and Binding Energies ΔE_{bind} for Zeolite−Guest Complexes[a]

	toluene		phenol	
method	$\Delta\varepsilon$ (kcal/mol)	ΔE_{bind} (kcal/mol)	$\Delta\varepsilon$ (kcal/mol)	ΔE_{bind} (kcal/mol)
RHF	0.	−8.0	0.	−16.5
AFO/*F*10	2.8	−12.1	7.8	−20.8
AFO/*F*9a	4.1	−10.0	7.2	−18.9
AFO/*F*9b	6.7	−8.2	10.4	−18.2
AFO/*F*8	6.3	−7.8	9.6	−16.4
HOP/*F*10	177.9	−10.5	191.4	−17.7
HOP/*F*9a	147.1	−10.5	153.6	−19.3
HOP/*F*9b	179.1	−9.2	194.8	−14.4
HOP/*F*8	148.9	−8.8	156.9	−16.0

[a] *F*8, *F*9a, *F*b, and *F*10 are different fragmentation schemes described in the text. RHF/6-31G* structures were used.

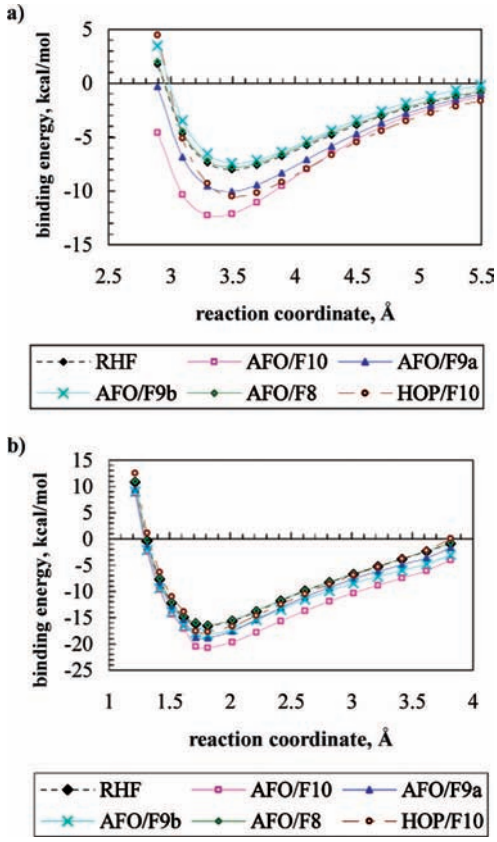

Figure 5. Energy profiles (6-31G*) for the adsorption of (a) toluene and (b) phenol on the faujasite zeolite surface, at different levels of FMO calculations (AFO and HOP), as well as ab initio RHF.

fragmentation can be seen. All schemes gave fairly reasonable binding energies, with errors of several kilocalories per mole at most. However, if a high accuracy is sought (such as when deciding where the preferable binding site is), a larger active-site fragment may be needed. For toluene it is clear that the addition of guest to the binding site fragment is more important than the binding site expansion (*F*9b vs *F*9a), but for phenol, which comes closer to zeolite, both factors are equally important, and when both are taken into account (*F*8), the error in the binding energy becomes very small (AFO, 0.2 and 0.1 kcal/mol for toluene and phenol, respectively; HOP, 0.8 and 0.5 kcal/mol, respectively).

The adsorption energy profiles are depicted in Figure 5. All curves resemble each other, being nearly parallel, indicating that various fragmentation schemes in FMO work reasonably well, with the errors being about 1−4 kcal/mol for both toluene and phenol. AFO/*F*10 apparently has the largest deviation from RHF in both cases. For phenol, AFO/*F*10, HOP/*F*10, and AFO/*F*9 feature a small unevenness in Figure 5b around 1.6 Å. On the contrary, AFO/*F*9b and AFO/*F*8 have smooth curves, which is because they include the guest molecule in the binding site fragment. It can also be seen in both cases that the latter two methods are the most reliable, almost exactly reproducing the RHF curve (which is nearly indistinguishable from RHF for AFO/*F*8).

Thus, including the adsorbant molecule with the binding site fragment gives very accurate binding energies and can be recommended to refine the final energetics. The downside of this usage is the inability to do the interaction analysis (Table 3), which applies to interfragment interactions; thus both schemes (such as *F*8 and *F*10) can be used for binding energies and interaction analysis, respectively. Practically, it is easy to switch to another scheme by a simple fragment assignment change in the calculation setup and redoing the computation.

Finally, we turn to future practical applications. The AFO scheme of bond division was shown to work reasonably well. However, it does not completely eliminate the problems of the dangling bond interaction, and the success of the zeolite fragmentation is partially due to the careful choice of fragmentation points avoiding close dangling bonds. It seems desirable to include the adsorbant molecule with the binding site fragment, and perhaps the rest of the fragmentation details are not very important as far as the binding energy is concerned; however, the remaining structure may be not unimportant, such as when comparing adsorption to different isomers (for the two faujasite zeolites in this work). Upon performing a fragmentation, one can look at ΔQ values and also at individual ΔQ_{IJ} terms to uncover potential problems.

4. Conclusions

By developing the new fragmentation scheme for the fragment molecular orbital method, we achieved a considerable expansion of its application field from mostly proteins, DNA, and molecular clusters into the industrially important field of catalysis and, possibly, surface chemistry. By careful comparison to the original method as well as to ab initio calculations, we demonstrated a considerable improvement in the description of polyalanine chains, and we identified problems with highly polar systems, such as proteins.

Application to the adsorption on the faujasite zeolite surface of the two adsorbant molecules showed that accurate binding energies (at most 0.2 kcal/mol error vs ab initio) can be achieved by careful fragmentation. Somewhat larger errors for the relative stability of the two faujasite zeolite isomers (3.4 kcal/mol) indicate that it may be useful to include three-body terms in the final energetics (FMO3) if such comparison is conducted.

For future development, the analytic gradient can be very useful for structure optimization. Recent advances[73] in the MP2 algorithms can be combined with our method, providing means to add the dispersion interaction to the binding energies. Also, the application of FMO to the calculation of chemical shifts[74] apparently suffered some accuracy loss from a distortion of the electronic structure in the vicinity of the detached bonds, and the application of AFO to NMR studies may be advantageous.

Acknowledgment. We thank Professor M. Suenaga of Kyushu University for developing his outstanding modeling software Facio, which is indispensable for easy fragmentation in FMO. D.G.F. and K.K. were partially supported by a Grant-

in-Aid for Scientific Research (JSPS, Japan) and the Next Generation SuperComputing Project, Nanoscience Program (MEXT, Japan). J.H.J. was supported by a Skou Fellowship from the Danish Research Agency (Forskningsrådet for Natur og Univers).

References and Notes

(1) Taylor, P. R. Accurate Calculations and Calibrations. In *European Summerschool in Quantum Chemistry*; Roos, B. O., Widmark, P.-O., Eds.; Lund University: Lund, Sweden, 2000; Book III, pp 641−711.

(2) Bytautas, L.; Matsunaga, N.; Nagata, T.; Gordon, M. S.; Ruedenberg, K. *J. Chem. Phys.* **2007**, *127*, 204313.

(3) Scuseria, G. E. *J. Phys. Chem. A* **1999**, *103*, 4782.

(4) Lee, M. S.; Maslen, P. E.; Head-Gordon, M. *J. Chem. Phys.* **2000**, *112*, 3592.

(5) Werner, H.-J.; Manby, F. R.; Knowles, P. J. *J. Chem. Phys.* **2003**, *118*, 8149.

(6) Nikitina, E.; Sulimov, V.; Zayets, V.; Zaitseva, N. *Int. J. Quantum Chem.* **2004**, *97*, 747.

(7) Sodt, A.; Subotnik, J. E.; Head-Gordon, M. *J. Chem. Phys.* **2006**, *125*, 194109.

(8) Nakajima, T.; Hirao, K. *Chem. Phys. Lett.* **2006**, *427*, 225.

(9) Paulus, B. *Phys. Rep.* **2006**, *428*, 1.

(10) Inaba, T.; Sato, F. *J. Comput. Chem.* **2007**, *28*, 984.

(11) Fedorov, D. G.; Kitaura, K. *J. Phys. Chem. A* **2007**, *111*, 6904.

(12) Kitaura, K.; Ikeo, E.; Asada, T.; Nakano, T.; Uebayasi, M. *Chem. Phys. Lett.* **1999**, *313*, 701.

(13) (a) Fedorov, D. G.; Kitaura, K. In *Modern Methods for Theoretical Physical Chemistry and Biopolymers*; Starikov, E. B., Lewis, J. P., Tanaka, S., Eds.; Elsevier: Amsterdam, 2006; pp 3−38. (b) Nakano, T.; Mochizuki, Y.; Fukuzawa, K.; Amari, S.; Tanaka, S. In *Modern Methods for Theoretical Physical Chemistry and Biopolymers*; Starikov, E. B., Lewis, J. P., Tanaka, S., Eds.; Elsevier: Amsterdam, 2006; pp 39−52.

(14) Fedorov, D. G.; Kitaura, K. *J. Chem. Phys.* **2004**, *120*, 6832.

(15) Fedorov, D. G.; Kitaura, K. *J. Chem. Phys.* **2004**, *121*, 2483.

(16) Sugiki, S.-I.; Kurita, N.; Sengoku, Y.; Sekino, H. *Chem. Phys. Lett.* **2003**, *382*, 611.

(17) Fedorov, D. G.; Kitaura, K. *J. Chem. Phys.* **2005**, *122*, 054108.

(18) Fedorov, D. G.; Kitaura, K. *J. Chem. Phys.* **2005**, *123*, 134103.

(19) Mochizuki, Y.; Koikegami, S.; Amari, S.; Segawa, K.; Kitaura, K.; Nakano, T. *Chem. Phys. Lett.* **2005**, *406*, 283.

(20) Maezono, R.; Watanabe, H.; Tanaka, S.; Towler, M. D.; Needs, R. J. *J. Phys. Soc. Jpn.* **2007**, *76*, 064301.

(21) Chiba, M.; Fedorov, D. G.; Kitaura, K. *J. Chem. Phys.* **2007**, *127*, 104108.

(22) Fedorov, D. G.; Kitaura, K.; Li, H.; Jensen, J. H.; Gordon, M. S. *J. Comput. Chem.* **2006**, *27*, 976.

(23) Fedorov, D. G.; Ishida, T.; Kitaura, K. *J. Phys. Chem. A* **2005**, *109*, 2638.

(24) Fedorov, D. G.; Olson, R. M.; Kitaura, K.; Gordon, M. S.; Koseki, S. *J. Comput. Chem.* **2004**, *25*, 872.

(25) Mochizuki, Y.; Yamashita, K.; Murase, T.; Nakano, T.; Fukuzawa, K.; Takematsu, K.; Watanabe, H.; Tanaka, S. *Chem. Phys. Lett.* **2008**, *457*, 396.

(26) Nakanishi, I.; Fedorov, D. G.; Kitaura, K. *Proteins: Struct., Funct., Bioinf.* **2007**, *68*, 145.

(27) Ito, M.; Fukuzawa, K.; Mochizuki, Y.; Nakano, T.; Tanaka, S. *J. Phys. Chem. A* **2008**, *112*, 1986.

(28) Watanabe, T.; Inadomi, Y.; Fukuzawa, K.; Nakano, T.; Tanaka, S.; Nilsson, L.; Nagashima, U. *J. Phys. Chem. B* **2007**, *111*, 9621.

(29) Komeiji, Y.; Ishida, T.; Fedorov, D. G.; Kitaura, K. *J. Comput. Chem.* **2007**, *28*, 1750.

(30) Mochizuki, Y.; Komeiji, Y.; Ishikawa, T.; Nakano, T.; Yamataka, H. *Chem. Phys. Lett.* **2007**, *437*, 66.

(31) Ishida, T.; Fedorov, D. G.; Kitaura, K. *J. Phys. Chem. B* **2006**, *110*, 1457.

(32) Mochizuki, Y.; Nakano, T.; Amari, S.; Ishikawa, T.; Tanaka, K.; Sakurai, M.; Tanaka, S. *Chem. Phys. Lett.* **2007**, *433*, 360.

(33) Mochizuki, Y.; Tanaka, K.; Yamashita, K.; Ishikawa, T.; Nakano, T.; Amari, S.; Segawa, K.; Murase, T.; Tokiwa, H.; Sakurai, M. *Theor. Chem. Acc.* **2007**, *117*, 541.

(34) Chiba, M.; Fedorov, D. G.; Kitaura, K. *J. Chem. Phys.* **2007**, *127*, 104108.

(35) Chiba, M.; Fedorov, D. G.; Kitaura, K. *J. Comput. Chem.*, DOI: 10.1002/jcc.21000.

(36) Fedorov, D. G.; Ishida, T.; Uebayasi, M.; Kitaura, K. *J. Phys. Chem. A* **2007**, *111*, 2722.

(37) Komeiji, Y.; Nakano, T.; Fukuzawa, K.; Ueno, Y.; Inadomi, Y.; Nemoto, T.; Uebayasi, M.; Fedorov, D. G.; Kitaura, K. *Chem. Phys. Lett.* **2003**, *372*, 342.

(38) Sato, M.; Yamataka, H.; Komeiji, Y.; Mochizuki, Y.; Ishikawa, T.; Nakano, T. *J. Am. Chem. Soc.* **2008**, *130*, 2396.

(39) Schmidt, M. W.; Baldridge, K. K.; Boatz, J. A.; Elbert, S. T.; Gordon, M. S.; Jensen, J. H.; Koseki, S.; Matsunaga, N.; Nguyen, K. A.; Su, S.; Windus, T. L.; Dupuis, M.; Montgomery, J. A. *J. Comput. Chem.* **1993**, *14*, 1347. GAMESS can be downloaded from http://www.msg.chem.iastate.edu/gamess/gamess.html.

(40) Suenaga, M. *J. Comput. Chem. Jpn.* **2008**, *7*, 33 (in Japanese). Facio 11.8.1 is available at http://www1.bbiq.jp/zzzfelis/Facio.html.

(41) Zhanpeisov, N. U.; Anpo, M. *J. Am. Chem. Soc.* **2004**, *126*, 9439.

(42) Zhanpeisov, N. U.; Fukumura, H. *J. Phys. Chem. C* **2007**, *111*, 16941.

(43) Zhao, Y.; Truhlar, D. G. *J. Phys. Chem. C* **2008**, *112*, 6860.

(44) Svensson, M.; Humbel, S.; Froese, R. J.; Matsubara, T.; Sieber, S.; Morokuma, K. *J. Phys. Chem.* **1996**, *100*, 19357.

(45) Jansang, B.; Nanok, T.; Limtrakul, J. *J. Phys. Chem. C* **2008**, *112*, 540.

(46) Maseras, F.; Morokuma, K. *J. Comput. Chem.* **1995**, *16*, 1170.

(47) Shoemaker, J. R.; Burggraf, L. W.; Gordon, M. S. *J. Phys. Chem. A* **1999**, *103*, 3245.

(48) Choi, C. H.; Liu, D.-J.; Evans, J. W.; Gordon, M. S. *J. Am. Chem. Soc.* **2002**, *124*, 8730.

(49) Cho, J.; Choi, C. H. *J. Phys. Chem. C* **2008**, *112*, 6907.

(50) Imamura, A.; Aoki, Y.; Maekawa, K. *J. Chem. Phys.* **1991**, *95*, 5419.

(51) Zhang, R.; Tian, W. Q.; Gu, F. L.; Aoki, Y. *J. Phys. Chem. C* **2007**, *111*, 6350.

(52) Willnauer, C.; Birkenheuer, U. *J. Chem. Phys.* **2004**, *120*, 11910.

(53) Pidko, E. A.; Mignon, P.; Geerlings, P.; Schoonheydt, R. A.; van Santen, R. A. *J. Phys. Chem. C* **2008**, *112*, 5510.

(54) Ishikawa, T.; Mochizuki, Y.; Imamura, K.; Nakano, T.; Mori, H.; Tokiwa, H.; Tanaka, K.; Miyoshi, E.; Tanaka, S. *Chem. Phys. Lett.* **2006**, *430*, 361.

(55) Corma, A. *Chem. Rev.* **1995**, *95*, 559.

(56) Mravec, D.; Zavadan, P.; Kaszonyi, A.; Joffre, J.; Moreau, P. *Appl. Catal., A* **2004**, *257*, 49.

(57) Borodina, I. B.; Pomakhina, E. B.; Ramishvili, Ts. M.; Ponomareva, O. A.; Rebrov, A. I.; Ivanova, I. I. *Russ. J. Phys. Chem.* **2006**, *80*, 892.

(58) Nakano, T.; Kaminuma, T.; Sato, T.; Akiyama, Y.; Uebayasi, M.; Kitaura, K. *Chem. Phys. Lett.* **2000**, *318*, 614.

(59) Gao, J.; Truhlar, D. G. *Annu. Rev. Phys. Chem.* **2002**, *53*, 467.

(60) Friesner, R. A.; Guallar, Y. *Annu. Rev. Phys. Chem.* **2005**, *56*, 389.

(61) Gordon, M. S.; Freitag, M. A.; Bandyopadhyay, P.; Jensen, J. H.; Kairys, V.; Stevens, W. J. *J. Phys. Chem. A* **2001**, *105*, 293.

(62) Smith, T.; Slipchenko, L. V.; Gordon, M. S. *J. Phys. Chem. A* **2008**, *112*, 5286.

(63) Kairys, V.; Jensen, J. H *J. Phys. Chem. A* **2000**, *104*, 6656.

(64) The Wired Chemist data base: http://www.wiredchemist.com/chemistry/data/bond_energies_lengths.html.

(65) Fedorov, D. G.; Kitaura, K. *Chem. Phys. Lett.* **2004**, *389*, 129.

(66) Edmiston, C.; Ruedenberg, K. *Rev. Mod. Phys.* **1963**, *35*, 457.

(67) Bode, B. M.; Gordon, M. S. *J. Mol. Graphics Modell.* **1998**, *16*, 133. MacMolPlot 7.2 is available at http://www.scl.ameslab.gov/∼brett/MacMolPlt/.

(68) Nemoto, T.; Fedorov, D. G.; Uebayasi, M.; Kanazawa, K.; Kitaura, K.; Komeiji, Y. *Comput. Biol. Chem.* **2005**, *29*, 434.

(69) Fedorov, D. G.; Kitaura, K. *J. Comput. Chem.* **2007**, *28*, 222.

(70) Fedorov, D. G.; Kitaura, K. *Chem. Phys. Lett.* **2006**, *433*, 182.

(71) Mo, Y.; Gao, J.; Peyerimhoff, S. D. *J. Chem. Phys.* **2000**, *112*, 5530.

(72) Kitaura, K.; Morokuma, K *Int. J. Quantum Chem.* **1976**, *10*, 325.

(73) Fedorov, D. G.; Ishimura, K.; Ishida, T.; Kitaura, K.; Pulay, P.; Nagase, S. *J. Comput. Chem.* **2007**, *28*, 1476.

(74) Gao, Q.; Yokojima, S.; Kohno, T.; Ishida, T.; Fedorov, D. G.; Kitaura, K.; Fujihira, M.; Nakamura, S. *Chem. Phys. Lett.* **2007**, *445*, 331.

JP805435N